University of Waterloo
Faculty of Science

ARIEL Basement-2 Level Beamline Commissioning Results

TRIUMF,
Vancouver, BC, V6T 2A3, Canada

Prepared by
Maire Bleszynski
20657295
3A Mathematical Physics

Monday 16th December, 2019

Abstract

This report will discuss progress of preliminary commissioning results on the ARIEL basement-2 level beamline path through the High Resolution Separator (HRS). This report will evaluate the efficacy of beam envelope models and tomography reconstruction by comparison with direct measurement. After analyzing the quality of measurement data, noise filtration algorithms, and reconstruction output, this study finds that initial reconstruction results look promising for calibration purposes, but current methods could be made more robust and accurate. There is demonstrable need for more a robust noise filtration algorithm in order to handle worst-case data sets taken by sub-optimal diagnostic machines in addition to enhancing the quality of typical data sets.

Acknowledgements

I would like to thank the following people for their guidance and advice; My supervisor, the beam physics group leader Rick Baartman, and the engineering physics group leader Marco Marchetto. They have helped me enormously by providing necessary beam physics knowledge, and by providing useful resources for this report including internal TRIUMF documents, schematics, technical manuals and design documentation. I would like to additionally acknowledge Spencer Kiy, Olivier Shelbaya, Thomas Planche, Jedri Deluna and Paul Jung for their assistance with the High Level Application (HLA) environment, their collaborative efforts in software projects, and especially, for their guidance and expertise.

Table of Contents

List of Tables

List of Figures

Glossary

beamline Cylindrical metal pipe, evacuated to high vacuum to prevent beam loss by scattering with air molecules 1

emittance Measure of average beam spread in position-and-momentum phase space 4, 7

isobaric Thermodynamic process in which the pressure remains constant. This is usually obtained by allowing the volume to expand or contract in such a way to neutralize any pressure changes that would be caused by heat transfer 1

isotope Subspecies of a single element differentiated by neutron number 1

profile monitor Measures current and voltage of a beam to generate a size and shape profile 6

quadrupole Generates electrostatic fields to deflect ion trajectories based on m/z values. Used for transverse focusing of beams. 4

Abbreviations

ARIEL Advanced Rare IsotopE Laboratory 1

ATIS ARIEL Test Ion Source 1

CANREB CANadian Rare Isotope facility with Electron Beam ion source 1

HLA High Level Application iii

HRS High Resolution Separator ii, 1

ISAC Isotope Separator and Accelerator 1

LEBT Low Energy Beam Transport 6

MENT Maximum ENTropy solution 7

RMS Root Mean Square 4, 5

Chapter 1

Introduction

The Advanced Rare IsotopE Laboratory (ARIEL) facility will effectively triple isotope production for TRIUMF's Isotope Separator and Accelerator (ISAC) experimental facilities with the addition of two new production stations and a new beamline transport system spanning 200 metres over three stories. Preliminary commissioning of new transport infrastructure in CANadian Rare Isotope facility with Electron Beam ion source (CANREB)[1] began in the ARIEL ground level in February 2019 and proceeded to the basement-2 level in September 2019. A test beam of cesium (+1) with an energy of 30keV was sent from the ARIEL Test Ion Source (ATIS) through the HRS to calibrate parameters related to the installation and function of beam delivery infrastructure. The ATIS should be capable of producing stable beams with an energy up to 60 keV.

---

[1] "CANREB will complement the presently used [Electron Resonance Cyclotron Ion Sources (ECRIS)] based charge state breeder system by providing higher purity beams and extending the available mass range. Ions are first sent through a high resolution mass separator, where most of the isobaric contaminants can be removed." (Ames, 2018)[1]

Beam parameter	HRS	RFQ/Buncher	RIB Beamline
Beam species	Rb^+ or Cs^+, K^+	Cs^+, Rb^+, K^+, Na^+, Li^+	Cs^+
Beam energy (E)	10.0 keV – 60.0 keV	10.0 keV – 60.0 keV	10.0 keV – 60.0 keV
Energy spread (ΔE) [4rms]	< 0.7 eV	< 10 eV	< 10 eV
Emit. (ε) at 60 keV [4rms]	< 6.0 μm	< 12.0 μm	< 12.0 μm
Beam intensity (I)	1 nA – 100 nA	100 fA – 100 nA	1 nA – 100 nA

Figure 1.1: Summary of basic beam requirements
Table 1 from the ATIS Design Note Document.[13](Saminathan,2017)
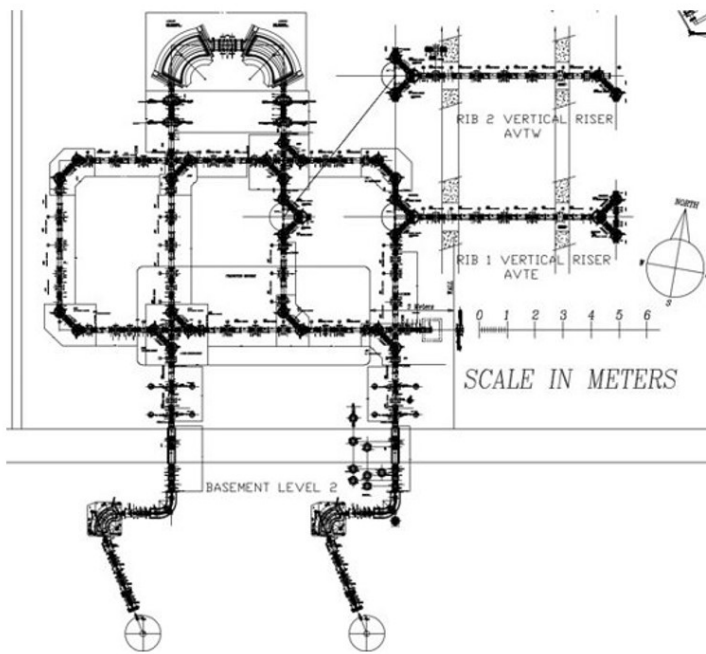
Figure 1.2: ARIEL B2 Layout

Chapter 2

Methods and Materials

2.1 Beam Envelopes

A beam envelope describes the transverse optics of the beam as a whole. The beam envelope is characterized by quadrupole focusing strengths and by initial conditions such as energy, particle mass, charge, current, Root Mean Square (RMS) and emittance (ϵ).
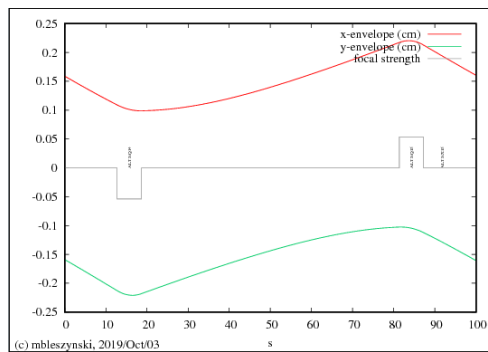
Figure 2.1: TRANSOPTR Beam Envelope Calculation

4

2.1 depicts a beam envelope calculated in TRANSOPTR[3] FORTRAN code. TRANSOPTR is based on older program, TRANSPORT[1]. The horizontal axis is distance along the beamline in centimetres and the vertical axis is twice the RMS (2ϵ) distance from the reference z-axis along the beamline to the approximate edge of the beam[2] in the x,y cross-sectional axes.[2] Match points are points along the beam-path where beam characteristics are consistent and calibrated by direct measurement. Profile monitors at these match points can collect current-voltage scans to reconstruct the RMS directly.

---

[1]"TRANSPORT is a first-and second-order matrix multiplication computer program intended for the design of static-magnetic beam transport systems."(Brown, 1983)[4]

[2]Beams do not have a physical edge in a meaningful sense. The area encompassing about 90% of particles is $4\pi\epsilon$

2.1.1 Wire Scanners
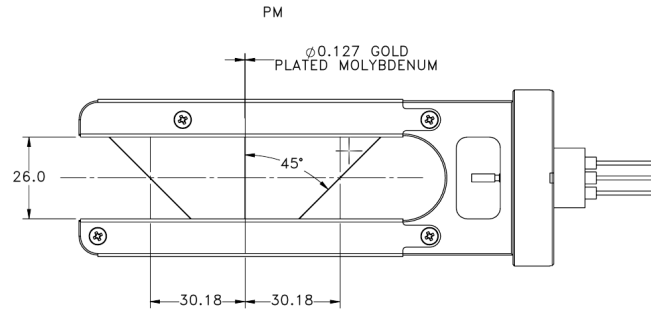
Figure 2.2: Wire Scanner Diagram

"Diagnostic devices are required to determine the ion beam profile, transverse beam position, beam intensity, emittance and pulse length of a transport beam through the ARIEL LEBT[3] beamline. Diagnostic devices also cut and shape the beam through attenuators, fixed-width collimators, and adjustable slits" (Planche, 2017)[14]

Wire scanners were chosen to fulfil ARIEL's specific design specifications. Wire scanners are a type of profile monitor that collects current along X, Y and mixed plane axes of the beam cross section. Position isn't measured directly with wire scanners, unlike profile monitors used elsewhere in TRIUMF facilities. Rotating profile monitors (RPMs), for example, work by collecting secondary emission from a grounded scanning wire. RPMs encode position implicitly. Wire scanners, on the other hand, measure voltage which can be converted to cross sectional positions by a measured conversion factor. This is a disadvantage to wire scanners as it introduces the possibility of miscalibration.

---

[3]Low Energy Beam Transport (LEBT)

2.2 Tomography Reconstruction

Tomography, in this context[4], is a process of constructing two-dimensional information from one-dimensional data. Beam physicists use tomography to extract useful beam parameters from simple one-dimensional beam profile scans. Phase space tomography can be used to reconstruct initial beam parameters such as emittance that are difficult to measure directly but encode essential properties of the beam. It is not possible to measure emittance directly in the ARIEL B2 level as there is presently no working emittance scanner installed. Furthermore, as emittance scanners are difficult to install, it is advantageous to avoid relying on them whenever possible. It is difficult to conduct phase space tomography successfully without a carefully calibrated data processing algorithm to satisfy the requirements for a reconstruction method (see below). That motivates a use for real space tomography as a calibration tool.

A real space tomography reconstruction extrapolates a beam intensity contour map from three position-current projections in the x, y and 45 degree xy plane. It is intuitive to understand this as an initial condition problem where supplying more initial conditions restricts degrees of freedom further and further. With only 3 projections, there is some ambiguity as to possible reconstruction solutions. This is essentially an optimization problem since the solution is not unique. An algorithm called Maximum ENTropy solution (MENT) converges to a solution that maximizes total entropy. This is, in theory, the most probable solution.

As previously mentioned, real space tomography is most applicable as a calibration tool

---

[4]More generally, how N-dimensional information can be extracted from lower-order projections.

for data processing algorithms because it is more straightforward in comparison to phase space tomography.

It is very practical to calibrate noise filtration and other forms of quality control with real space tomography because a single set of scan data will produce a reconstruction. This reconstruction process has been expedited by a web application tool, discussed further in section 2.4, to make the feedback process nearly instantaneous. The quality of input data, noise filtration, smoothing factors, and agreement between MENT input and output can be assessed by this method.

2.3 Tomography Calibration

There are several reasons why phase space reconstruction is difficult. First, it requires a multi-step scan process over a range of phase-angle rotations that encompasses the minimum beam size [12].
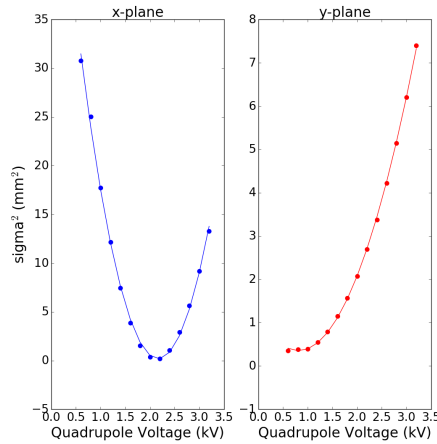
Figure 2.3: σ^2 vs Voltage

This is not always easy to achieve without compromising beam transmission or reaching quadrupole voltage setting limits. Secondly, the reconstruction is superbly sensitive to noise. Removing background noise with a low pass filter is a necessary first step, but not sufficient for all cases. A compromise must be found between the minimum amount of smoothing to allow the reconstruction algorithm to converge, and the threshold where useful information and detail is lost beyond recognition.

2.4 High Level Web Application Development

Although high level applications are by no means a perfect solution, they have proven effective in expediting the process of calibrating ARIEL B2 level diagnostics.

The addition of a new beam profile and tomography application allows TRIUMF operators to access and analyze diagnostic data live in the control room while initiating diagnostic scans. Recent scan data sets would suggest diagnostics are in good working order. Observed noise noise levels are sufficiently low enough for successful tomography reconstruction.(2.4)
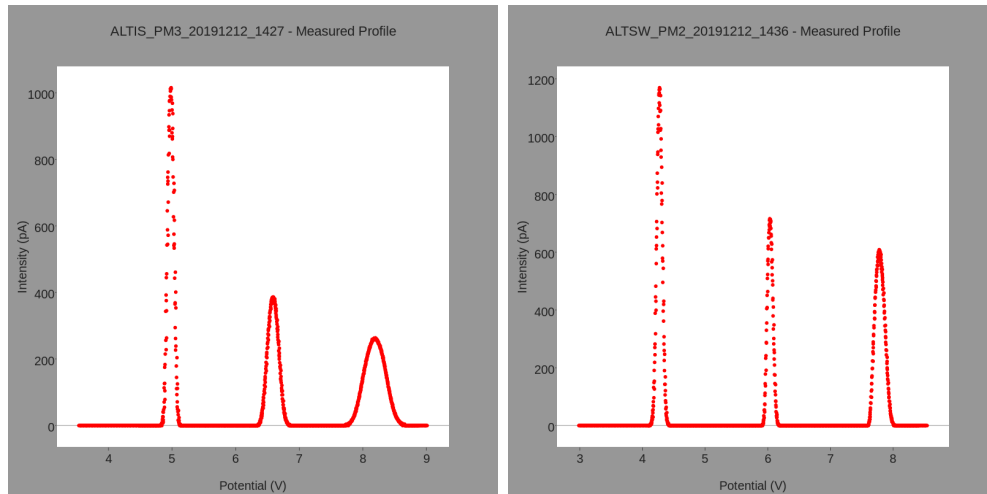
Figure 2.4: Current intensity (pA) vs voltage (V)
Measured data at locations ALTIS:PM3 and ALTSW:PM2.

The real space tomography web application was conceived as a compliment to a pre-existing phase space tomography application; an accessible web browser tool to be used during live scans in the control room. The real space tomography application would expedite the process of generating beam profiles from output data and performing real space tomography

10

in the browser. It has potential to offer valuable feedback to operators. Beam aberrations or diagnostic miscalibrations could be spotted far sooner. This application was used to generate figures 2.4, 3.1, 3.3, 3.2, 3.4, 4.1, and 4.2 using an open source plotting library called Plotly [11]. The data processing and reconstruction input files were generated by python scripts written by previous commissioning co-op students. [7] [8]

Chapter 3

Results and Analysis

3.1 Tomography

3.1.1 Real Space Reconstruction: Summary

Table 3.1 summarizes the results of tomography reconstructions generated using the real space tomography web application.

Diagnostic	Measured	Measured	Tomography	Tomography	$\|\frac{\check{X}-X}{X}\|$	$\|\frac{\check{Y}-Y}{Y}\|$	$\frac{\Delta X+\Delta Y}{2}$
-	2X RMS(mm)	2Y RMS(mm)	2X̃ RMS(mm)	2Ỹ RMS(mm)	ΔX	ΔY	-
ALTIS:PM3	1.17	3.90	1.40	3.90	19.7%	0.00%	9.85%
ALTS:PM7	2.51	2.49	2.53	2.47	0.80%	0.80%	0.80%
ALTSW:PM2	1.08	1.82	1.02	1.84	5.56%	1.10%	3.33%
ALTS:PM17	1.79	2.72	1.75	2.68	2.23%	1.47%	1.85
ALTW:PM39	1.75	2.01	1.30	2.03	25.7%	1.00%	13.35%

Table 3.1: Measured beam profiles and tomography reconstruction calculated profiles

3.1.2 Real Space Reconstruction: Plots

Left: Measured input versus MENT output

Right: MENT Reconstruction Intensity Contour Map
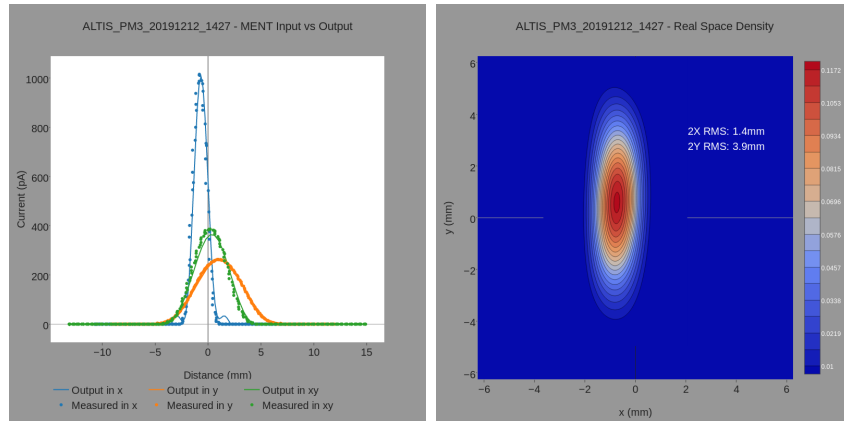
Figure 3.1: Real space reconstruction at location ALTIS:PM3
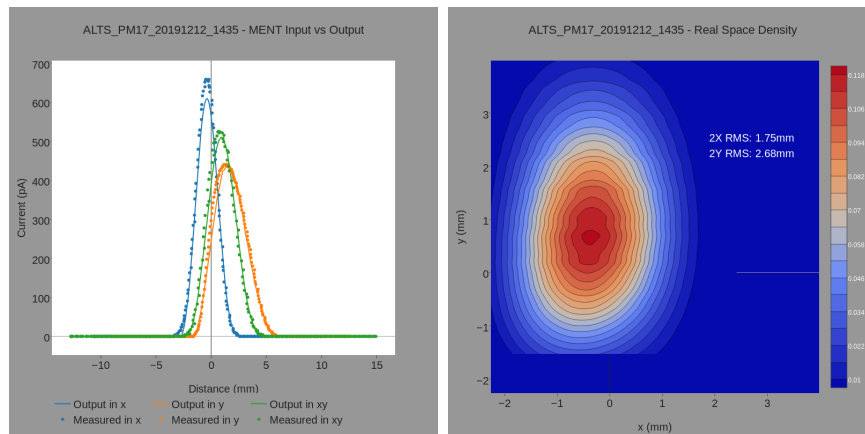
Figure 3.2: Real space reconstruction at location ALTS:PM17

13
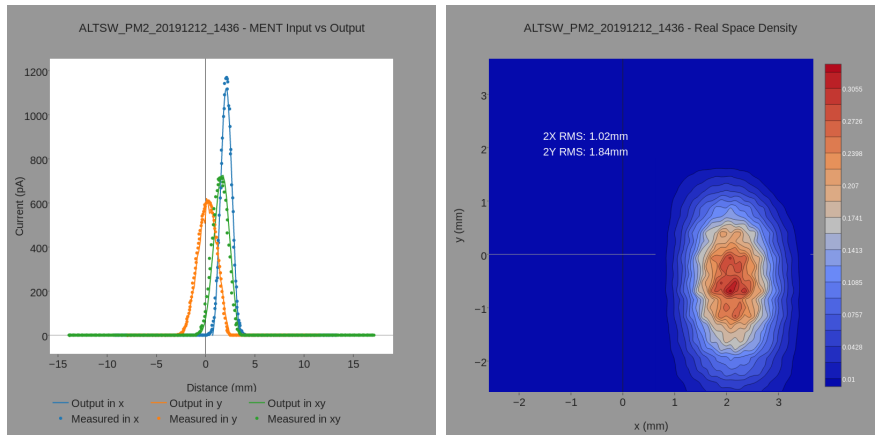
Figure 3.3: Real space reconstruction at location ALTSW:PM2
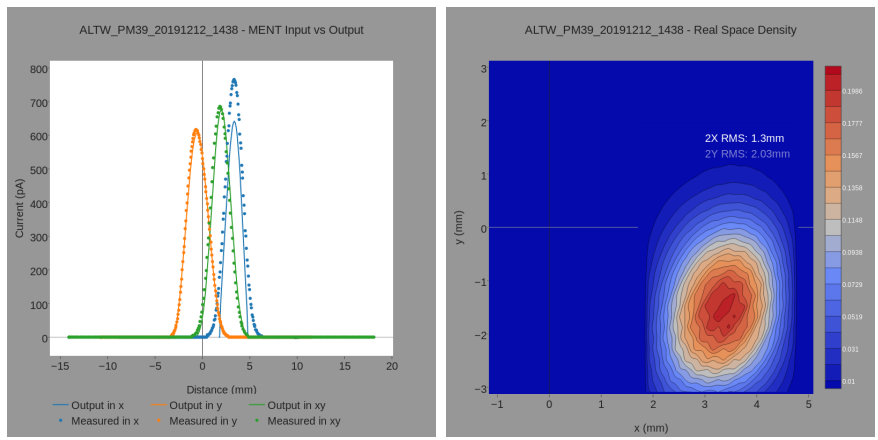
Figure 3.4: Real space reconstruction at location ALTW:PM39

3.1.3 Conversion Factor Calibration
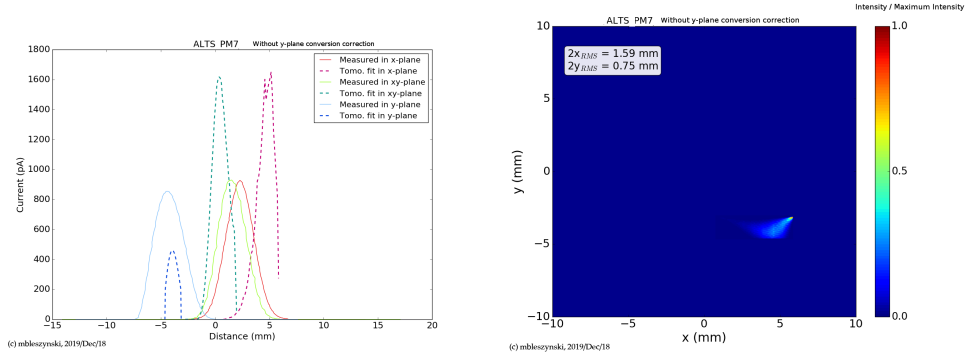
Figure 3.5: Real space reconstruction with miscalibrated conversion factor
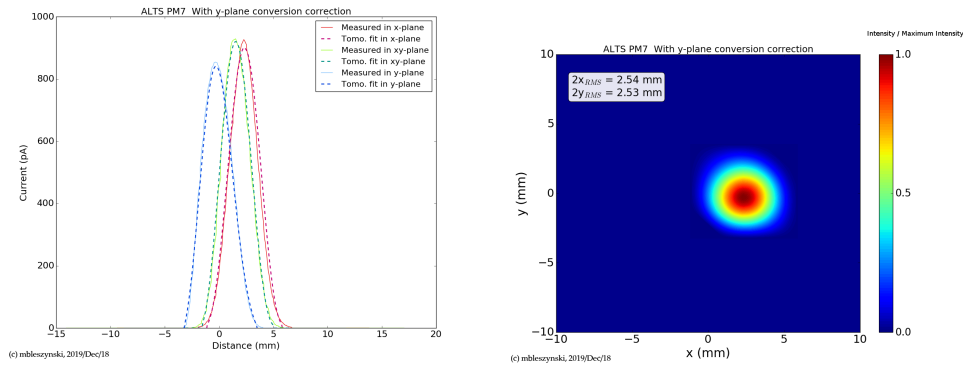
Figure 3.6: Real space reconstruction with recalibrated conversion factor

Figures 3.5 and 3.6 were plotted by python scripts. The first reconstruction failed to match the input and output parameters successfully because the profiles contained contradictory information. A miscalibration of the y-plane was found to be the cause. The y-plane centroid was roughly 5mm offset from its true position. After recalibrating the y-plane, the next reconstruction managed to match measurements within a margin of 0.80% (table 3.1).

3.1.4 Phase Space Reconstruction

Figures 3.7 and 3.8 were plotted by python scripts.

Two sets of scans were conducted at the ALTS:PM7 location in order to acquire sufficient data for a phase space reconstruction in the x and y planes. One quadrupole was held fixed while another varied over a range. The leftmost figures depict the measured input (solid lines) versus reconstructed output (dotted lines). The rightmost figures are MENT reconstruction intensity plots. These reconstructions were used to generate a beam envelope calculation from the location of measurement, ALTS:PM7. 3.10.

16
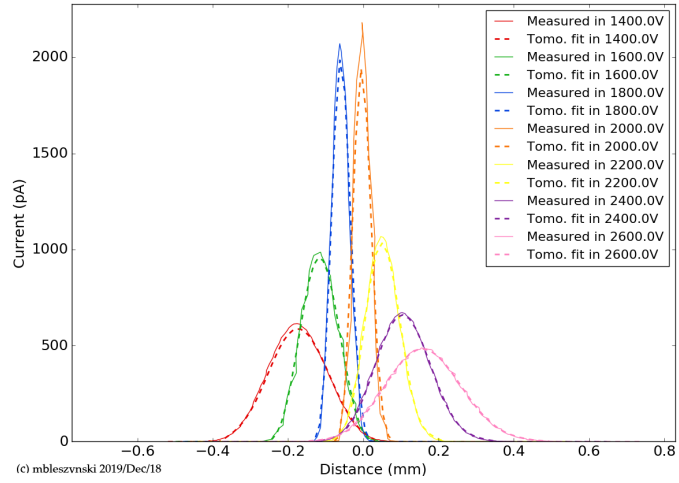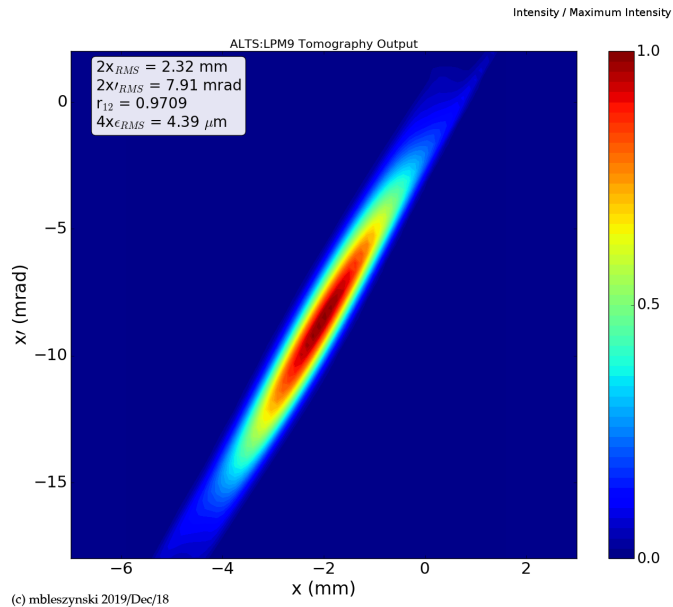
Figure 3.7: Phase Space Reconstruction along X plane
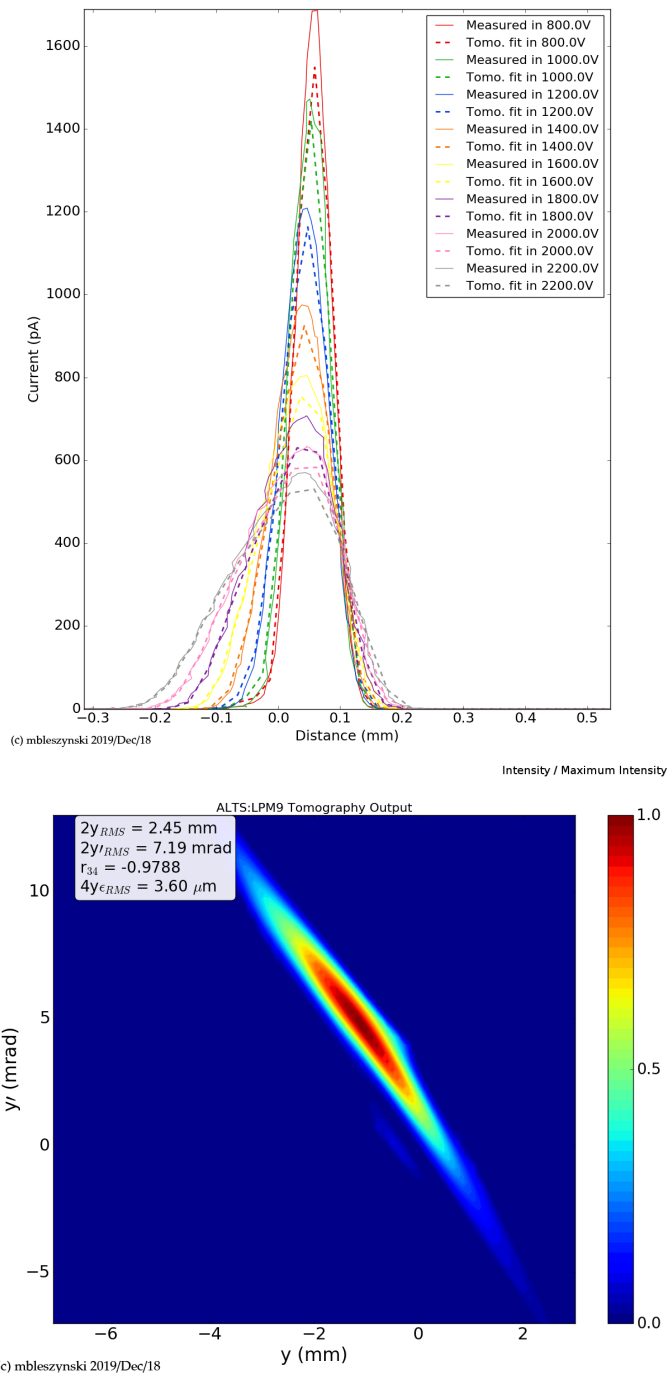
Figure 3.8: Phase Space Reconstruction along Y plane

3.2   Beam Envelope Calculations
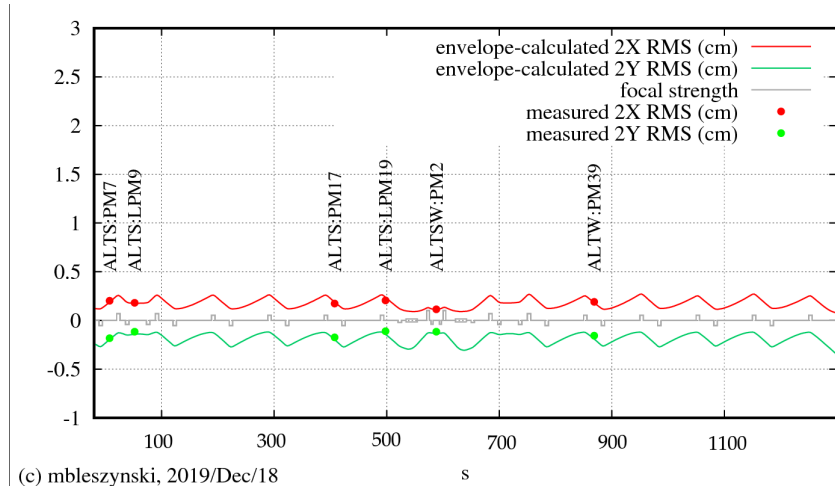
Figure 3.9: Theoretical envelope calculation vs match-point measurements
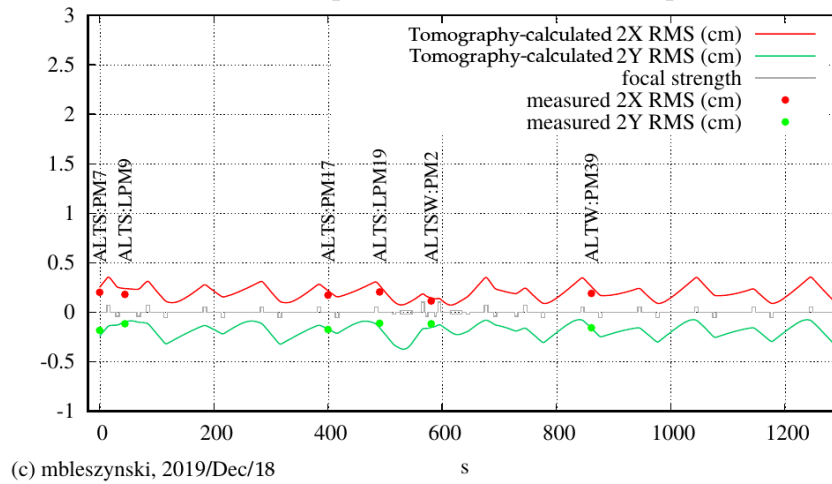
Figure 3.10: Phase reconstructed envelope calculation vs match-point measurements

Chapter 4

Discussion

4.1 Match-Point Conditions

As seen in figure 3.9 and table 3.1, imposed match point conditions agree with measurement within a margin of 1% or 0.02mm along x and y at the location of the wire scanner ALTS:PM7. The beamline installation process requires micrometer precision for most components, except the diagnostics. Operators have freedom to move diagnostics around as necessary, therefore a certain degree of positional uncertainty must be allowed for. This could account for a 1% margin of error in the estimated RMS values. Real space tomography reconstruction quality varies from less than a percent to roughly 13%, averaged over x and y. This is not unexpected since reconstruction quality is sensitive to noise. Nevertheless, this is acceptable for a minimally smoothed reconstruction method. Further study is needed to determine an optimal smoothing process.

4.2 Wire Scanner Calibration

Wire scanners come with disadvantages. A mis-calibrated measurement was found to be the cause of bad real space reconstruction at the location of a wire scanner ALTS:PM7 3.5. It can be seen in the highly truncated peaks and confirmed by a separate calculation that misplaces the y-axis wire by 5 milimetres. After corrections were made, good reconstruction was achieved.

4.3 Tomography Reconstruction Algorithm

Tomography reconstructions often require fine-tuned smoothing[1] for particularly noisy data sets. One solution is to tweak the internal smoothing algorithm MENT uses, by a variable factor, for each particular data set. This is not ideal for several reasons. First, the amount of smoothing needed varies between profile monitors and particular data sets. The MENT smoothing algorithm does not calibrate itself; the user must choose an appropriate smoothing factor. Second, MENT smoothing can destroy too much information. It would be better not to use MENT smoothing at all, but instead use a more reliable and predictable smoothing algorithm to ensure that bias and data loss are transparent. Let's see an example data set where minimal smoothing is insufficient for an accurate reconstruction.

---

[1]A technique of eliminating noise from a dataset while preserving large-scale structure. Many types of algorithms can accomplish this.
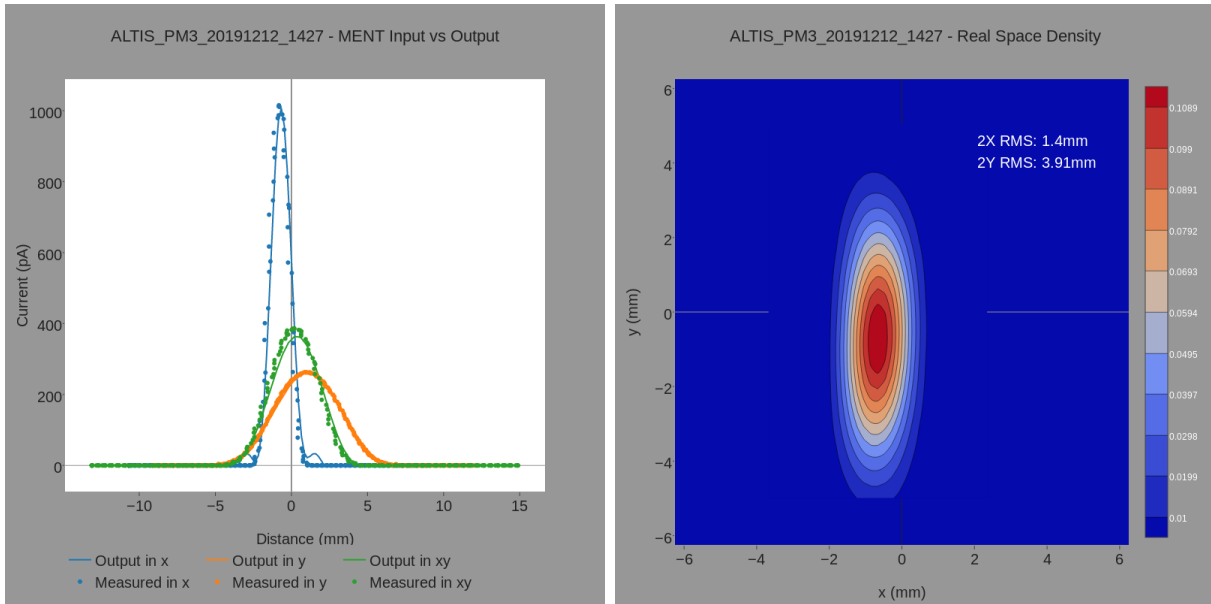
Figure 4.1: Real Space Reconstruction with Smooth-factor=3
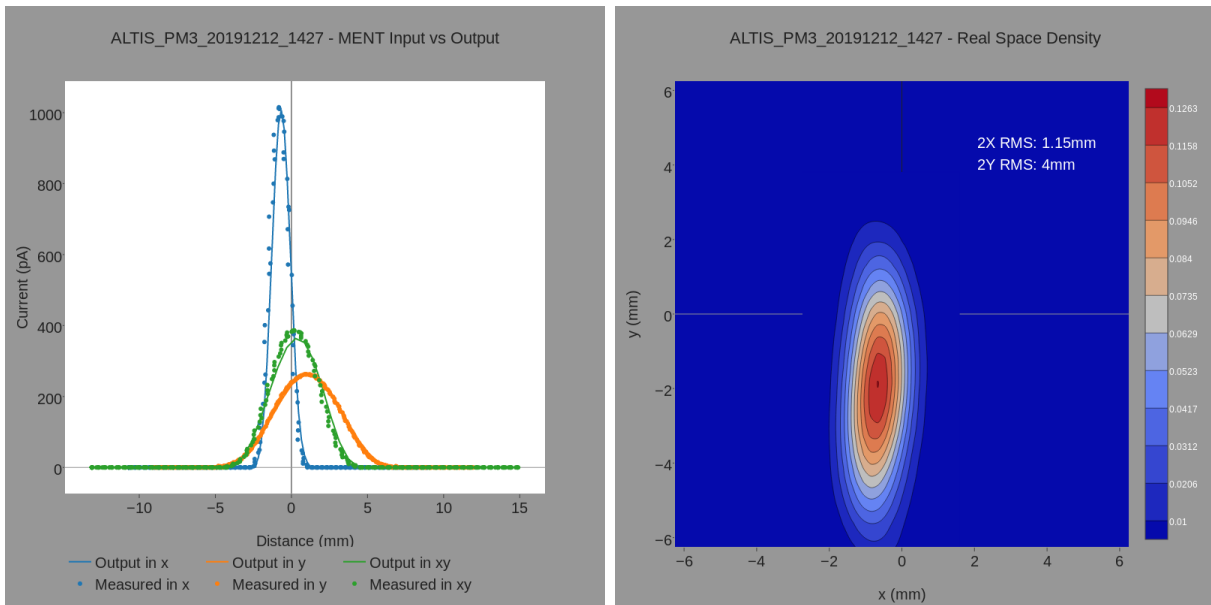
Figure 4.2: Real Space Reconstruction with Smooth-factor=4

In 4.1, notice the extra bump present in the tails of the x-plane peak. This feature is evidence that the MENT algorithm has not converged to an accurate solution, possibly due to irregular noise in the raw data. Further evidence for a poor reconstruction can be seen by the fact that 2X RMS disagrees with measurement (3.1) by 19.7%. After further smoothing the reconstruction seems to improve. The tail peak disappears and the 2x RMS is within 1.71%.

Chapter 5

Conclusion

5.1 Summary

Thus far, real space tomography results look promising. This study finds good agreement between reconstruction and measurement. Basement-2 level diagnostics exhibit good working condition with consistently low noise levels. Initial phase space tomography reconstruction scans at the location of profile monitor ALTS:PM7 are promising; in fact, emittance is within the expected range for a 30KeV beam.[13] Reconstruction quality could be improved by better data processing algorithms.

5.2   Recommendations

There are many types of smoothing algorithms that could be adapted to suit our requirements.

Recommendation 1: Median smoothing is a common non-linear filtering technique [15] in digital signal processing. Median smoothing is effective for removing impulse or 'spiky' noise, of short duration. There is an abundance of documentation for median smoothing and various libraries such as SciPy[16] support it.

Recommendation 2. LULU smoothing is another non-linear filtering technique comparable to median smoothing. LULU smoothing has the advantage of idempotence over median smoothing. Indempotence means that no further smoothing takes place beyond the initial application because the root signal is identified and preserved. [6]

References

[1] F. Ames, R. Baartman, B. Barquest, C. Barquest, M. Blessenohl, J. R. Crespo López-Urrutia, J. Dilling, S. Dobrodey, L. Graham, R. Kanungo, M. Marchetto, M. R. Pearson, and S. Saminathan. The canreb project for charge state breeding at triumf. *AIP Conference Proceedings*, 2011(1):070010, 2018.

[2] R. Baartman. Emittance Convention . Technical Report TRI-BN-15-07, TRIUMF, June 2015.

[3] R. Baartman. `TRANSOPTR`: Changes since 1984. Technical Report TRI-BN-16-06, TRIUMF, 2016.

[4] Karl L Brown. First-and second-order matrix theory for the design of beam transport systems and charged particle spectrometers. Technical report, Stanford Linear Accelerator Center, Calif., 1971.

[5] D. Gray and B. Minato. Simple "package design" ion chamber monitors for triumf's proton beamlines. In *AIP Conference Proceedings*, volume 648, pages 439–446. AIP, 2002.

[6] Maria Dorothea Jankowitz. *Some statistical aspects of LULU smoothers*. PhD thesis, Stellenbosch: University of Stellenbosch, 2007.

[7] O. Lailey. Tomography Reconstruction for ARIEL CANREB Beam Commissioning. Technical Report TRI-BN-19-07, TRIUMF, 2019.

[8] A. Mahon and S. Saminathan. Preliminary CANREB Beamline Comissioning Results. Technical Report TRI-BN-19-19, TRIUMF, 2019.

[9] J. A. Maloney, M. Marchetto, and R. Baartman. ARIEL High Resolution Separator. Technical Report TRI-DN-14-06, TRIUMF, 2014.

[10] M. Marchetto and S. Saminathan. ARIEL Front-End. Technical Report Document-41767, TRIUMF, 2016.

[11] Plotly, Inc. Plotly graphing libraries.

[12] Yi-Nong. Rao. Maximum Entropy Tomography Validation. Technical Report TRI-BN-18-16, TRIUMF, 2018.

[13] Suresh Saminathan. ARIEL Test Ion Source. Technical Report TRI-DN-16-35, TRIUMF, 2017.

[14] P.̃Jung T.̃Planche. Relativistic Lagrangian and Hamiltonian Description of a Beam with Space-Charge. Technical Report TRI-BN-17-05, TRIUMF, 2017.

[15] John W Tukey. *Exploratory data analysis*, volume 2. Reading, Mass., 1977.

[16] Pauli Virtanen, Ralf Gommers, Travis E. Oliphant, Matt Haberland, Tyler Reddy, David Cournapeau, Evgeni Burovski, Pearu Peterson, Warren Weckesser, Jonathan Bright, Stéfan J. van der Walt, Matthew Brett, Joshua Wilson, K. Jarrod Millman, Nikolay Mayorov, Andrew R. J. Nelson, Eric Jones, Robert Kern, Eric Larson, CJ Carey, İlhan Polat, Yu Feng, Eric W. Moore, Jake Vand erPlas, Denis Laxalde, Josef Perktold, Robert Cimrman, Ian Henriksen, E. A. Quintero, Charles R Harris, Anne M. Archibald, Antônio H. Ribeiro, Fabian Pedregosa, Paul van Mulbregt, and SciPy 1. 0 Contributors. SciPy 1.0–Fundamental Algorithms for Scientific Computing in Python. *arXiv e-prints*, page arXiv:1907.10121, Jul 2019.